

Article

Application of Dithiocarbamate Chitosan Modified SBA-15 for Catalytic Reductive Removal of Vanadium(V)

Yilin Huang ¹, Jia Wang ^{2,3,*} , Mengwei Li ¹ and Zhixiong You ^{1,*}¹ School of Resource and Environmental Sciences, Wuhan University, Wuhan 430072, China² School of Environmental Science and Engineering, Huazhong University of Science and Technology, Wuhan 430074, China³ Key Laboratory of Material Chemistry and Service Failure, School of Chemistry and Chemical Engineering, Huazhong University of Science and Technology, Wuhan 430074, China

* Correspondence: jiawang@hust.edu.cn (J.W.); zyou@whu.edu.cn (Z.Y.); Tel.: +86-027-87734899 (Z.Y.)

Abstract: We have successfully synthesized dithiocarbamate chitosan modified SBA-15 (CS₂C@SBA) composites, with promise in vanadium (V(V)) elimination. Among the three composites using different mass ratios of dithiocarbamate chitosan to SBA-15, CS₂C@SBA–3, which had the highest CS₂ substitution, showed the best performance on V(V) removal of which the maximum adsorption capacity could achieve 218.00 mg/g at pH 3.0. The adsorption kinetics were best fitted with a pseudo–second order reaction model, suggesting a chemisorption mechanism. Meanwhile, the Langmuir model fitted better with the adsorption isotherm, revealing a monolayer adsorption behavior. Through FTIR and XPS analysis, the functional group –SH was identified as dominating reduction sites on this composite, which reduced 73.1% of V(V) into V(IV) and V(III). The functional group –NH– was the main adsorption site for vanadium species. This reaction followed a catalytic reduction coupled adsorption mechanism reducing most of V(V) into less toxic vanadium species. Furthermore, CS₂C@SBA–3 showed great selectivity towards V(V) in the presence of various co–existing ions in synthetic wastewater and real water samples. Moreover, CS₂C@SBA–3 could retain a removal efficiency over 90% after five adsorption–desorption cycles. Based on the aforementioned results, we can conclude that CS₂C@SBA–3 has great potential to be applied in efficient remediation of vanadium water–pollution.

Keywords: vanadium elimination; adsorption; catalytic reduction; thiol function group; dithiocarbamate chitosan modified SBA-15



Citation: Huang, Y.; Wang, J.; Li, M.; You, Z. Application of Dithiocarbamate Chitosan Modified SBA-15 for Catalytic Reductive Removal of Vanadium(V). *Catalysts* **2022**, *12*, 1469. <https://doi.org/10.3390/catal12111469>

Academic Editors: Jiangkun Du, Lie Yang and Chengdu Qi

Received: 27 October 2022

Accepted: 15 November 2022

Published: 18 November 2022

Publisher's Note: MDPI stays neutral with regard to jurisdictional claims in published maps and institutional affiliations.



Copyright: © 2022 by the authors. Licensee MDPI, Basel, Switzerland. This article is an open access article distributed under the terms and conditions of the Creative Commons Attribution (CC BY) license (<https://creativecommons.org/licenses/by/4.0/>).

1. Introduction

Vanadium pollution has become a worldwide problem with the extending process of industrialization, such as steelmaking, battery manufacturing, and medicinal processing [1–3]. Vanadium is a potential toxic contaminant that may cause pulmonary tumors and oxidative cell damage if it is over ingested [4]. There exist various valence states of vanadium including +2, +3, +4 and +5 [5,6]. The higher the valence state of vanadium is, the more toxicity and stability it has [7]. Over the past, a variety of methods including ion exchange, surface complexation and electrostatic interaction have been applied for the elimination of V(V). Anion exchange resins such as D201, D314 and 711 were employed for the removal of V(V), achieving a removal efficiency up to 99.0% [8]. *Lactococcus raffinolactis* was proved to have promising prospects in the elimination of V(V), offering microbial resources for the bioremediation of a V(V)–polluted environment [9]. Among aforementioned traditional technologies for the remediation of V(V), adsorption was the most widely used, due to its high removal efficiency and low cost. For example, surface modified pine bark was investigated with the maximum adsorption capacity of 35.00 mg/g with quaternary nitrogen groups on its surface as the dominant adsorption sites [10]. Kong et al. synthesized a double hydroxide–supported nanoscale zero–valent iron (nZVI@LDH)

for the elimination of vanadium, which achieved the maximum adsorption capacity of 93.70 mg/g at initial pH of 3.0 [11].

Chitosan is a natural and linear copolymer comprised of β -(1,4)-glucopyranose units containing randomly distributed N-acetyl-glucosamine and glucosamine residues [12,13]. The application of pristine chitosan to the removal of heavy metals is limited by its low surface area and restricted accessibility of surface functional groups [14,15]. Thus, various physical and chemical synthetic methods have been adopted to modify chitosan into more application-worthy composites with improved adsorption properties [16–18]. Due to the presence of abundant heteroatoms and polar functional groups serving as potential complexation sites with metal ions, derivatives of chitosan can be considered as potential remediation agents for the elimination of heavy metals [19]. A dithiol functional terminal may be introduced to chitosan (CS₂-chitosan) [20]. The successfully grafted thiol functional groups (-SH) may then serve as reactive sites to reduce vanadium at high valence states into lower valence states. It is well known that the -SH/-SS- redox couple displays a standard oxidation potential of 0.420 V [21,22], while the standard reduction potential of a V(V/IV) couple is 1.420 V [23]. Thus, thiol groups (-SH) are a promising reducing site theoretically to donate electrons to V(V). Furthermore, the abundance of -NH₂ and -OH may promote the adsorption process due to their coordination with V(V). Thus, CS₂-chitosan may preclude the desorption of vanadium species back into the water matrix due to its folded configuration. Applications of chitosan alone may be limited in neutral or alkaline conditions by the difficulty of convoluted separation procedures, since it is hydrophobic in nature [24]. Thus, coating CS₂-chitosan on a stable support may be feasible to synthesize a promising heterogeneous adsorbent for practical applications to the remediation of vanadium contaminated wastewater. As is acknowledged, Santa Barbara Amorphous type 15 material (SBA-15) is one of the most popular support materials for the development of heterogeneous composites in which the 2D hexagonal array of uniformly distributed mesopores plays a vital role in the easy diffusion of substrate molecules [25]. Due to the distinctive properties, high surface area and abundance of hydroxyl groups on its surface [26], SBA-15 can compensate for the disadvantages of CS₂-chitosan, facilitating the rafting of polymers.

Inspired by the aforementioned facts, we proposed a dithiocarbamate chitosan modified SBA-15 (CS₂C@SBA) composite as a heterogeneous remediation agent for the catalytic reduction coupled adsorption of V(V) in this work. During this research, we investigated the impacts of various parameters including pH value, the dosage of CS₂C@SBA, contact time, initial concentration of V(V) and co-existing anions on the elimination of V(V). Afterwards, recycling and regeneration studies were carried out. As the mechanism of catalytic reduction of V(V) by -SH functional groups is not clear, a series of characterization techniques such as Fourier transform infrared spectroscopy (FTIR), scanning electron microscope combined with an electron dispersive X-ray (SEM-EDS) and X-ray photoelectron spectroscopy (XPS) were employed to analyze the change of the physicochemical properties of CS₂C@SBA before and after the reaction. Three CS₂C@SBA materials with distinct ratios of SBA-15 and modified dithiocarbamate chitosan were tested to disclose the structure-performance relationships. Finally, the performance was tested in real waters to further evaluate the potential of CS₂C@SBA in future practical applications. By all the aforementioned efforts, we aim to shed light on the adsorption and catalytic reduction mechanism of V(V) by CS₂C@SBA, and to confirm the potential of its future applications.

2. Result and Discussion

2.1. Structural Characterizations of Modified CS₂C@SBA-1,2,3

Three CS₂C@SBA materials which were synthesized with the mass ratios of CS₂-chitosan to SBA-15 of 2:1, 1:1 and 1:2 were named as CS₂C@SBA-1, CS₂C@SBA-2 and CS₂C@SBA-3, respectively. The elemental compositions of the synthesized materials, which were confirmed by elemental analyzer, are listed in Table 1. The elemental contents of N (weight percentage) of CS₂C@SBA-1, CS₂C@SBA-2 and CS₂C@SBA-3 were 4.50%, 3.52% and 2.62%, while the

contents of S were 1.97%, 1.73% and 1.36%, respectively (Table 1). To calculate the CS₂ substitution, the corresponding results of CS₂C@SBA-1, CS₂C@SBA-2 and CS₂C@SBA-3 were 19.19%, 21.52% and 22.72%, respectively (Table 1). Among the three CS₂C@SBA, the CS₂ substitution of CS₂C@SBA-3 was the highest, which indicated that more -CS₂ functional groups (22.76%) are grafted with CS₂C@SBA-3 composites (Table 1). FTIR spectra also suggested that the -CS₂ functional groups were fabricated on the surface successfully. The obvious bands at 1084 and 783 cm⁻¹ were the asymmetric and symmetric stretching of Si-O-Si, respectively, reflecting the successful hybridization of CS₂-chitosan and SBA-15 (Figure 1A) [26]. The bands stretching at 3454, 2920, 2873, 1629 and 1465 cm⁻¹ represented the existence of -OH/-NH₂/-SH, -CH₃, -CH₂, -CNH, and -C=S (Figure 1A) [20,27–29], respectively, which were same as the stretching bands in the FTIR spectra of CS₂-chitosan. Additionally, the intensities of those bands increased along with the increase of the amount of CS₂ substitution. The band intensities of asymmetric and symmetric stretching of Si-O-Si increased along with the increase of mass ratio of SBA-15. The pH_{ZPC} of SBA-15 and CS₂-chitosan were determined as 7.7 and 6.0, respectively (Figure 1B). With the hybrid of SBA-15 and CS₂chitosan, the pH_{ZPC} of CS₂C@SBA-3 changed into 6.9 (Figure 1B). XPS survey spectra (Figure 1C) of CS₂C@SBA-3 before the reaction were consistent with the results of elemental analysis (Table 1). All the signals of O, N, C, S and Si were found. XPS spectra of CS₂C@SBA-3 confirmed the existence of sulfur signals at the binding energies of 161.7 and 162.8 eV, which indicated the presence of -C=S and -CS- functional groups, respectively (Figure 1D) [30]. According to these characterization results, we can conclude that the CS₂chitosan was successfully fabricated on the surface of SBA-15.

Table 1. Elemental composition of synthesized materials.

Adsorbent	Elemental Composition ^a (wt%)				Degree of CS ₂ Substitution (%)
	C	H	N	S	
SBA-15	0.09	1.17	0.03	0.01	NA
CS ₂ Chitosan	42.54	7.42	7.92	3.92	20.96
CS ₂ C@SBA-1	32.83	6.21	4.50	1.97	19.19
CS ₂ C@SBA-2	25.40	5.35	3.52	1.73	21.52
CS ₂ C@SBA-3	18.99	4.21	2.62	1.36	22.72

^a Determined through elemental analysis. NA: Not applicable.

The physical properties of SBA-15 and CS₂C@SBA-3 are shown in Table S1 and Figure S1. As the successful hybrid of CS₂-chitosan, the Brunauer-Emmett-Teller (BET) surface areas of SBA-15 and CS₂C@SBA-1, CS₂C@SBA-2 and CS₂C@SBA-3 were calculated as 632.6, 121.4, 223.4 and 309.2 m²/g (Table S1), respectively. The BET surface area increased with the increasing mass ratio of CS₂-chitosan to SBA-15. Furthermore, the pore width increased from 2.04 to 2.28 nm while the pore volume increased from 0.1637 to 0.1762 cm³/g, respectively (Table S1 and Figure S1). CS₂C@SBA was mainly micro-mesopore structure (>2 nm). The X-ray diffraction (XRD) patterns revealed the ordered mesoporous structure of SBA-15 and CS₂C@SBA-3 (Figure S2). The peak at 23° was assigned for the amorphous SiO₂. Typical peaks at 0.8° (100), 1.6° (110) and 1.8° (200) indicated the mesopore structure of SBA-15 [31–34]. Furthermore, SEM images (Figure 2A–F) clearly showed the surface morphology of SBA-15, CS₂-chitosan and CS₂C@SBA-3 [35,36]. In the SEM image of CS₂C@SBA-3, it can be found that SBA-15 was uniformly wrapped by CS₂-chitosan (Figure 2E,F). To sum up, all the analyses above from the different characterizations proved the coating of CS₂-chitosan on the surface of SBA-15 [37]. TEM images (Figure S3) of SBA-15 exhibited cylindrical silicate layer morphologies [21,35]. After reaction with CS₂-chitosan, TEM images of CS₂C@SBA-3 (Figure S3) exhibited a core-shell structure which indicated the successful hybrid of CS₂-chitosan and SBA-15 [21]. Besides, after the reaction with V(V), CS₂-chitosan was still coated on the surface of SBA-15 (Figure S4). The phenomena suggested a robust nature of CS₂C@SBA-3 in the adsorption coupled catalytic reduction processes.

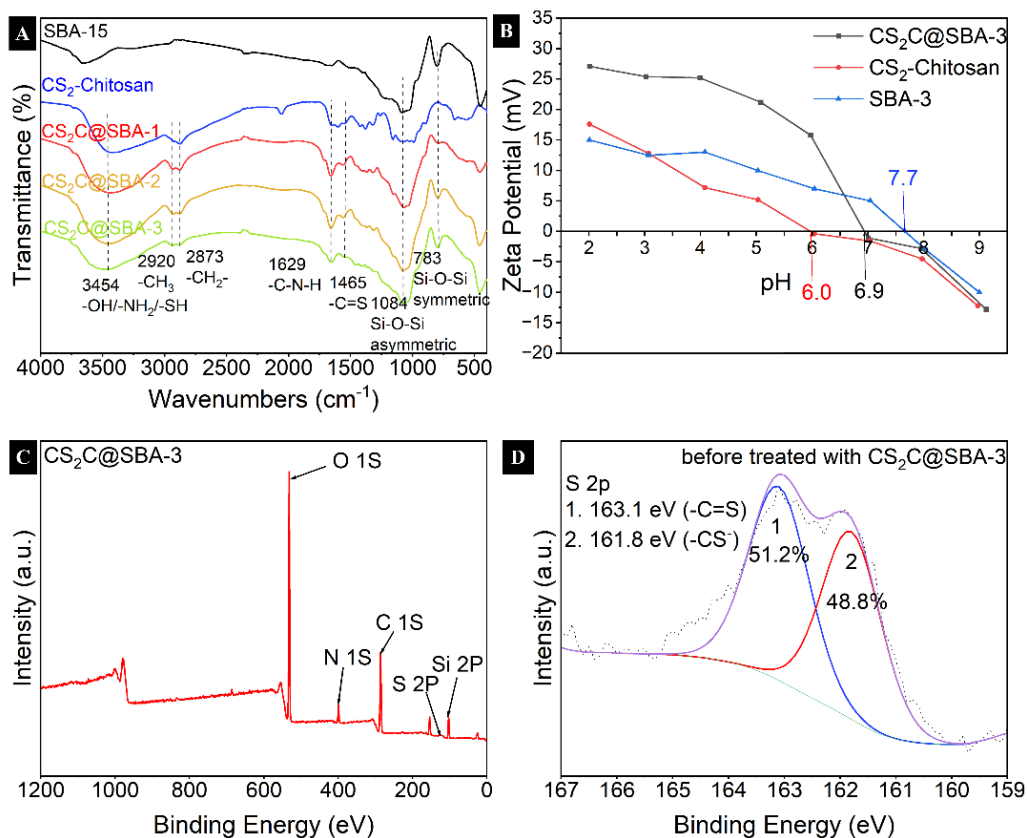


Figure 1. FTIR spectra of synthesized composites (A); Zeta potential plots of SBA-15, CS₂-chitosan and CS₂C@SBA-3 (B). The XPS survey spectra of CS₂C@SBA-3 before reaction (C). High resolution XPS spectra S 2p of CS₂C@SBA-3 (D).

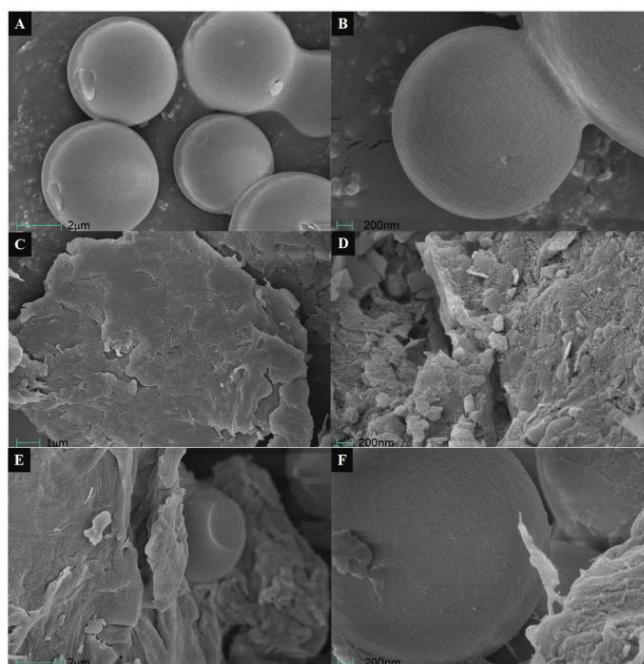


Figure 2. SEM images of SBA-15 (A,B); CS₂-chitosan (C,D); CS₂C@SBA-3 (E,F).

2.2. Adsorption Properties on Vanadium (V) Elimination

2.2.1. Effects of pH

The solution pH is one of the most important influence factors in the removal of heavy metal since it can change not only the surface charge properties of adsorbents but also the distribution of metal ions species [38,39]. As is acknowledged, the distribution of V(V) oxyanions exists in different forms at different solution pH values [40,41]. Taking those facts into consideration, we decided to determine the removal of V(V) by CS₂C@SBA-1, CS₂C@SBA-2 and CS₂C@SBA-3 at a specific pH ranging from 2.0 to 10.0.

Figure 3 showed the effects of pH value on the removal of V(V). CS₂C@SBA-1, CS₂C@SBA-2 and CS₂C@SBA-3 achieved V(V) removal of 62.2%, 72.1% and 98.2% at pH 3.0, respectively (Figure 3). CS₂C@SBA-3 demonstrated the highest efficiency in the removal of V(V). Furthermore, the removal of V(V) can be strongly influenced by the mass ratio of SBA-15/CS₂-chitosan. With the increase of SBA-15/CS₂-chitosan mass ratio, the removal efficiency was remarkably enhanced since there were more functional groups grafted on the surface of the composites, which acted as reactive sites to remove V(V). However, the removal efficiency of V(V) by CS₂C@SBA-3 decreased from 98.2% to 4.6% with the increase of solution pH from 2.0 to 10.0, while it decreased from 62.2% and 72.1% to 4.5% and 4.6% for CS₂C@SBA-1 and CS₂C@SBA-2, respectively (Figure 3). Hence, the optimum pH value for the removal of V(V) was determined as 3.0. The p*H*_{ZPC} of CS₂C@SBA-3 is 6.9 (Figure 1B) which suggested a negative surface charge at pH over 6.9 and a positive surface charge at pH under 6.9. Vanadium anions were reported to mainly exist as H₂V₁₀O₂₈⁴⁻, H₂VO₄⁴⁻ and H₃V₁₀O₂₈³⁻ at pH 3.0 [2]. Therefore, positively charged CS₂C@SBA-3 should have an electrostatic attraction with V(V) oxyanions at solution pH 3.0, favoring the adsorption of V(V) oxyanions. The analysis above suggests a strong co-relationship between pH value and the removal of V(V). An acidic environment favored the immobilization of V(V) by CS₂C@SBA-3.

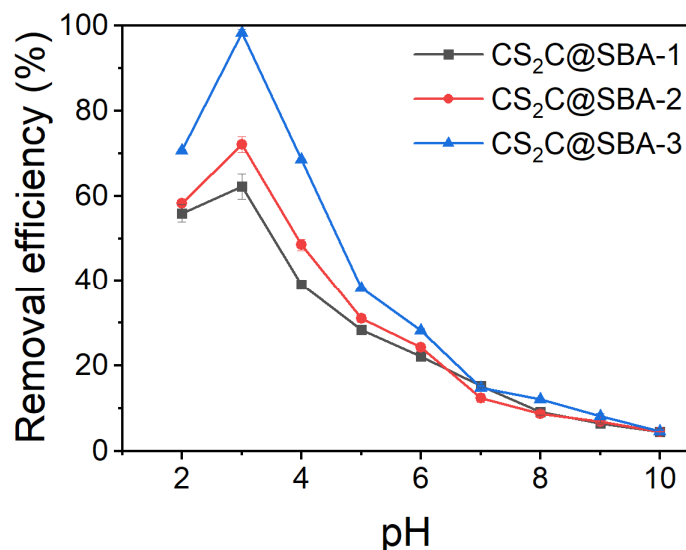


Figure 3. Effects of pH on V(V) elimination. Conditions: V(V) initial concentration = 100 ppm, CS₂C@SBA dosage = 1.0 g/L, experimental temperature = 298 K, contact time = 24 h.

2.2.2. Effects of the Dosage of CS₂C@SBA-3

To determine the effects of the dosage of CS₂C@SBA-3, a series of different dosages were examined in a 100 ppm V(V) solution. As the dosage increased from 0.1 to 2.0 g/L, the removal efficiency of V(V) increased from 31.2% to 99.7% (Figure 4). This might be attributed to the increase of the density of reactive sites on the surface. However, the removal efficiency of V(V) increased only slightly with increases in dosage from 1.0 to 1.5 and 2.0 g/L. The phenomena suggested that the removal of V(V) attained an equilibrium with the dosage of CS₂C@SBA-3 higher than 1.0 g/L. Thus, the adsorption

capacity decreased from 312.44 to 49.85 mg/g along with the increase of the dosage of CS₂C@SBA-3 (Figure 4). The moles ratio of V(V) to CS₂C@SBA-15 is inadequate at higher adsorbent dosages, indicating that the reactive sites on the surface of CS₂C@SBA-3 did not reach saturation point in those cases.

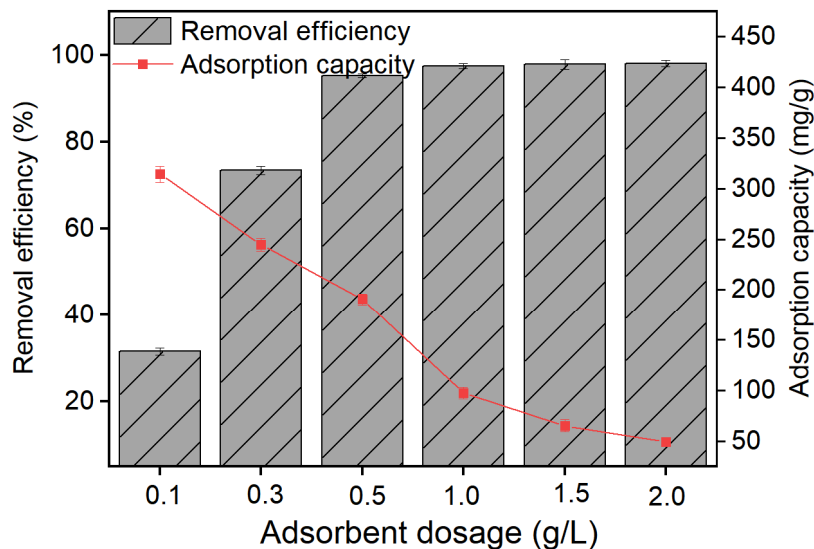


Figure 4. Effects of the dosage of CS₂C@SBA-3 on the removal of V(V). Conditions: V(V) initial concentration = 100 ppm, pH value = 3.0, experimental temperature = 298 K, contact time = 24 h.

2.3. Adsorption Kinetics

Figure 5A–C and Table 2 show the kinetics of the elimination of V(V). The effects of reaction time were investigated in a 100 ppm V(V) solution. Within the initial 5 min, 48.9% of V(V) was removed by CS₂C@SBA-3 (Figure 5A). The elimination rate was fast in the first 10 min. These results might be attributed to the abundance of reactive sites on the surface of CS₂C@SBA-3 which were quickly enriched with V(V). After 360 min of reaction, an equilibrium was reached, with 98.2% removal of V(V) due to the saturation of reactive sites (Figure 5A). Based on the data, the maximum adsorption capacity was calculated as 98.24 mg/g. The kinetics data were carefully fitted by both pseudo-first-order model and pseudo-second-order models. The regression coefficient (R^2) values of pseudo-second-order model were higher (0.9999) compared with pseudo-first-order model ($R^2 = 0.9851$) and Elovich model ($R^2 = 0.8788$) (Figure 5B–D). Hence, the pseudo-second-order kinetic model fitted better than the pseudo-first-order kinetic model and Elovich model did. The phenomena indicated that the elimination of V(V) by CS₂C@SBA-3 was primarily directed by the chemisorption [37,40,42,43].

Table 2. The parameters of kinetic and thermodynamics models for the adsorption of V(V) on CS₂C@SBA-3.

Models	Parameters	Parameters	Parameters
Pseudo-first-order model	K_1 (min^{-1})	Q_e ($\text{mg}\cdot\text{g}^{-1}$)	R^2
	0.014	39.813	0.9851
Pseudo-second-order model	K_2 ($\text{mg}\cdot\text{g}^{-1}\cdot\text{min}^{-1}$)	Q_e ($\text{mg}\cdot\text{g}^{-1}$)	R^2
	0.001	98.045	0.9999
Elovich model	α ($\text{mg}\cdot\text{min}\cdot\text{g}^{-1}$)	β ($\text{mg}\cdot\text{g}^{-1}$)	R^2
	41.341	9.057	0.8788
Langmuir model	Q_m ($\text{mg}\cdot\text{g}^{-1}$)	K_L ($\text{L}\cdot\text{mg}^{-1}$)	R^2
	221.193	0.260	0.9982
Freundlich model	n	K_f ($\text{mg}^{1-n}\cdot\text{L}^n\cdot\text{g}^{-1}$)	R^2
	4.252	65.663	0.9218

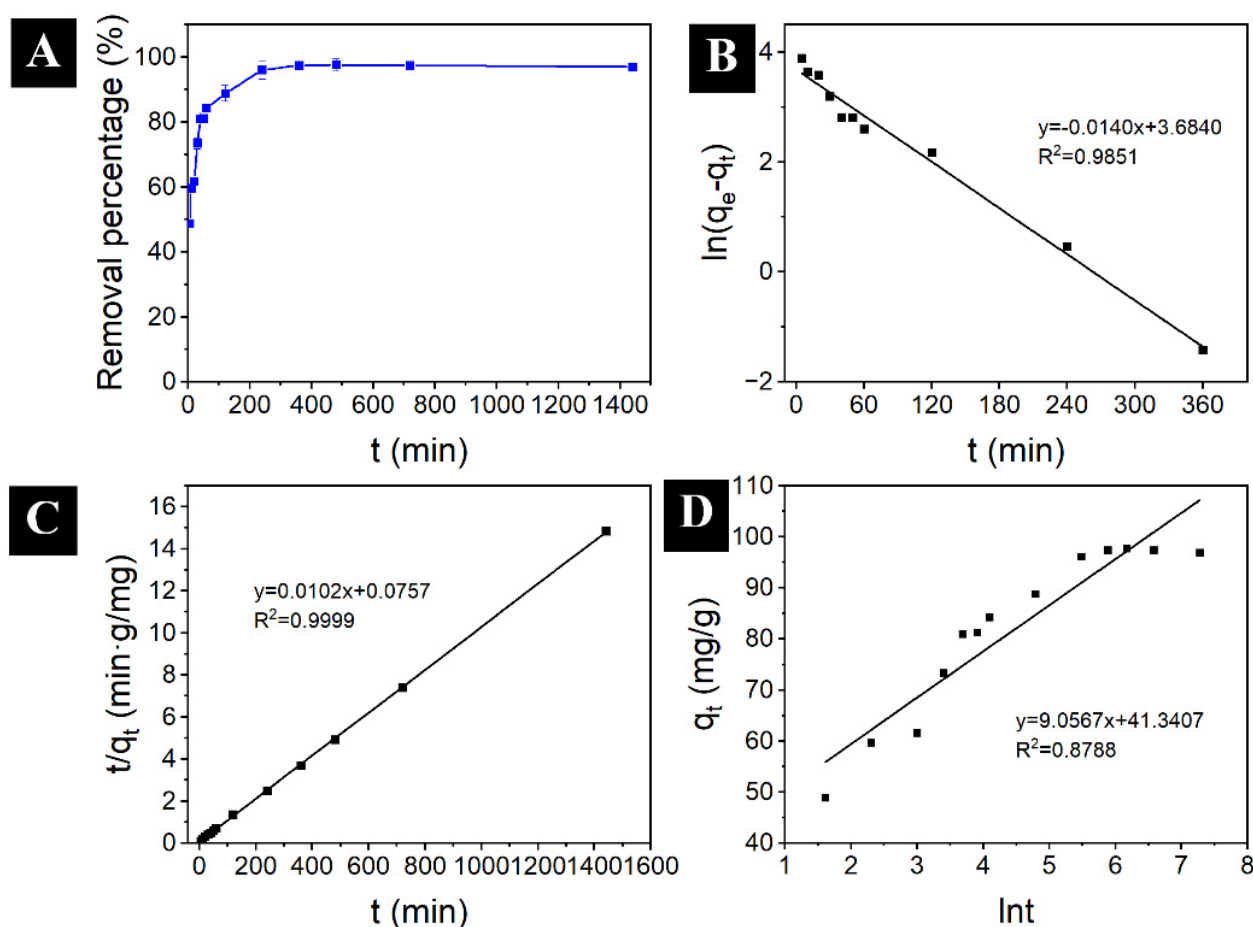


Figure 5. Kinetics studies. (A) V(V) removal percentage versus time; (B) fitted results for linearized pseudo–first order; (C) pseudo–second order kinetic models; and (D) Elovich model. Conditions: V(V) initial concentration = 100 ppm, CS₂C@SBA–3 dosage = 1.0 g/L, pH value = 3.0, experimental temperature = 298 K.

2.4. Adsorption Isotherm

To identify the adsorption interaction and the type of adsorption, adsorption isotherms were investigated at a series of initial V(V) concentrations (10–500 ppm). Figure 6 and Table 2 show the isotherm results of V(V) removal. The V(V) removal efficiency decreased from 98.6% to 43.6% while the adsorption capacity increased from 8.64 to 218.00 mg/g along with the increase of V(V) concentration from 10 to 500 ppm (Figure 6A). Two different isotherm models including Langmuir and Freundlich ones were used to fit the data [44,45]. From the parameters listed in Table 2, the Langmuir model fitted better than Freundlich models, since their correlation coefficient (R^2) were 0.9982 and 0.9218, respectively (Figure 6B and Table 2). From the calculation results of the Langmuir model, Q_m of CS₂C@SBA–3 is 221.19 mg/g which is appropriately equal to the measured experimental value (218.00 mg/g) (Table 2). The phenomena suggested that the adsorption of V(V) by CS₂C@SBA–3 was based on the assumption of monolayer distribution of V(V) on the surface of CS₂C@SBA–3 and no lateral interaction between V(V) and CS₂C@SBA–3 [46,47]. As long as a molecule occupies the reactive site on CS₂C@SBA–3, there is no adsorption that can take place at this site any more.

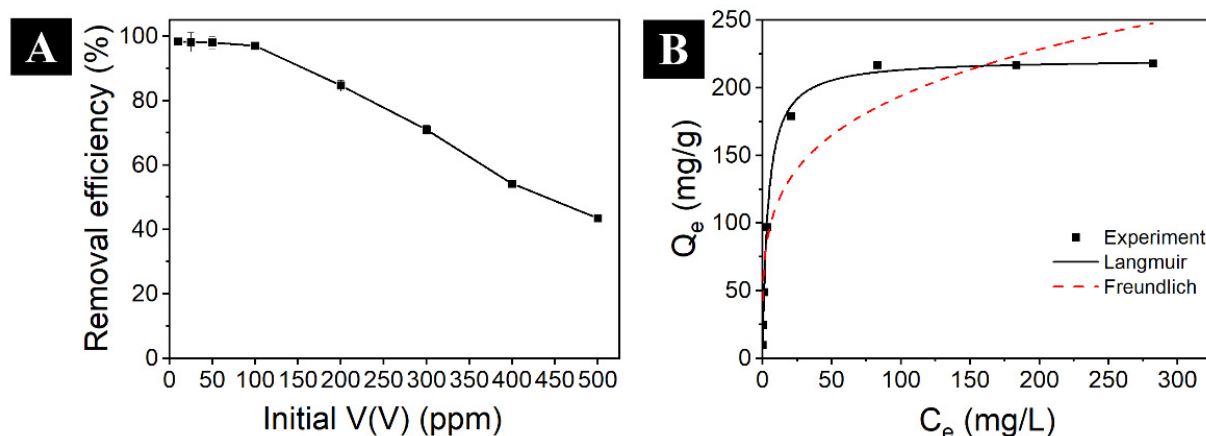


Figure 6. Isotherm studies. (A) removal efficiency versus V(V) initial concentration, (B) adsorption capacity versus equilibrium concentration. Conditions: $\text{CS}_2\text{C@SBA-3}$ dosage = 1.0 g/L, pH value = 3.0, experimental temperature = 298 K, contact time = 24 h.

2.5. Effects of Competing Anions

In real wastewater or groundwater, there are abundant co-existing anions which may have negative impacts on the removal of V(V). The co-existing anions may compete with V(V) for the reactive sites on the surface of composites. Thus, to simulate the real groundwater, the effects of co-existing anions (60 ppm PO_4^{3-} , 600 ppm SO_4^{2-} , 400 ppm NO_3^- , 400 ppm HCO_3^-) and 60 ppm Cu^{2+} and ionic strength (0.01, 0.1, and 0.3 M) on the removal of V(V) were studied [11,48].

Figure 7A,B indicate the impacts of various of co-existing anions and ionic strength on the elimination of V(V) by $\text{CS}_2\text{C@SBA-3}$. $\text{CS}_2\text{C@SBA-3}$ showed a predominant selectivity for the uptake of V(V). Despite of the presence of the competing anions, over 98.0% of V(V) could be removed from the solution except for two cases in the presence of 600 ppm SO_4^{2-} and 400 ppm HCO_3^- . The removal efficiency rates of V(V) were 95.9% and 97.2% in the presence of SO_4^{2-} and HCO_3^- , respectively (Figure 7A). This could be attributed to slight competition on reactive sites between V(V) and the two anions. Furthermore, the ionic strength demonstrated only slight impacts on the elimination of V(V) by $\text{CS}_2\text{C@SBA-3}$ because V(V) removal efficiency could achieve over 98.0% in a wide range of NaCl concentrations from 10 to 300 ppm (Figure 7B). All the aforementioned results suggest a promising performance of $\text{CS}_2\text{C@SBA-3}$ in the presence of common anions in wastewater or groundwater.

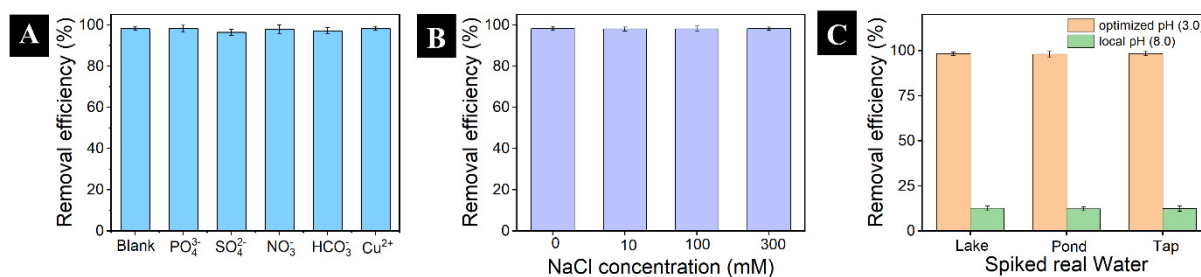


Figure 7. Effects of co-existing ions (A), effects of ionic strength (B) and the elimination of V(V) in real water samples (C). Conditions (A,B): V(V) initial concentration = 100 ppm V(V), and 60 ppm PO_4^{3-} , 600 ppm SO_4^{2-} , 400 ppm NO_3^- , 400 ppm HCO_3^- and 60 ppm Cu^{2+} , $\text{CS}_2\text{C@SBA-3}$ dosage = 1.0 g/L, experimental temperature = 298 K, contact time = 24 h; Condition(C): V(V) initial concentration = 10 ppm, $\text{CS}_2\text{C@SBA-3}$ dosage = 1.0 g/L, experimental temperature = 298 K, contact time = 24 h.

2.6. The Elimination of V(V) in Real Waters

In order to evaluate the practical potential of CS₂C@SBA-3, the elimination of V(V) was tested in three types of real water samples including lake, pond and tap waters. At pH 3.0, the removal efficiency of V(V) from lake, pond and tap waters was 99.5%, 99.8% and 99.3% respectively (Figure 7C). The results indicated that CS₂C@SBA-3 was highly efficient in real water bodies. However, V(V) removal efficiency by CS₂C@SBA-3 decreased to 77.5%, 75.2% and 75.4% in lake, pond and tap waters, respectively, at a local pH of 8.0 (Figure 7C). Hence, we can conclude that pH value has a significant impact on the removal of V(V), which was consistent with our previous results in Section 2.2.1. The dramatic decrease of V(V) removal may be attributed to the electrical repulsion between negatively charged CS₂C@SBA-3 and V(V) oxyanions at pH 8.0. The results suggest that CS₂C@SBA-3 can be successfully employed for the remediation of V(V) in real wastewater with appropriate adjustment of pH value.

2.7. Mechanism for V(V) Removal by CS₂C@SBA-3

SEM-EDS analysis was conducted to investigate the morphology and elemental composition of CS₂C@SBA-3 before and after the remediation of V(V). Figure 8A-E and Figure S4 show the structure and morphology of CS₂C@SBA-3 after the reaction. Comparing with Figure 2E,F, SBA-15 was still coated with CS₂-chitosan uniformly and there was nearly no obvious change on the morphology after treatment with 100 ppm V(V) for 24 h. Table 3, Figures S5 and S6 show the results of EDS elemental mapping of CS₂C@SBA-3 before and after the reaction. The results are consistent with the results of elemental analysis which can be considered as solid evidence supporting the successful complexation of the composites (Tables 1 and 3). Before the reaction, no signal of V was detected (Figure 8F). After treatment with large amounts of vanadium ions, CS₂C@SBA-15 was enriched with V which accounted for 12.2 wt% of the composite (Figure 8G and Table 3). The results once again indicated that large amounts of V(V) were adsorbed on the surface of CS₂C@SBA-3.

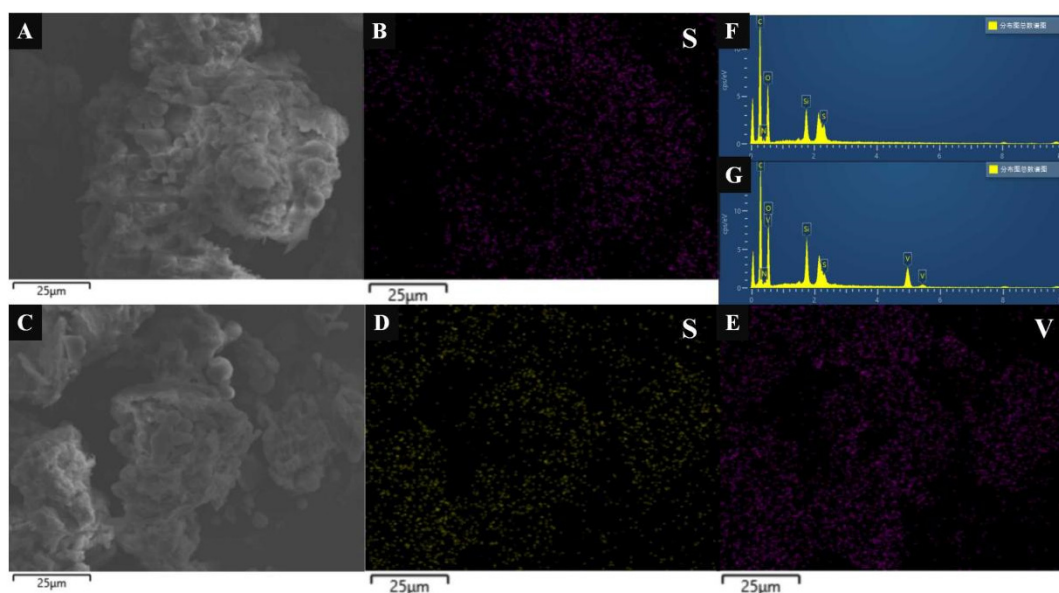


Figure 8. SEM-EDS images of CS₂C@SBA-3 before adsorption with V(V) (A) and EDS elemental mapping images (B,F), SEM-EDS images of CS₂C@SBA-3 after adsorption with V(V) (C) and EDS elemental mapping images (D,E,G). Conditions: Conditions: V(V) initial concentration = 100 ppm, CS₂C@SBA-3 dosage = 1.0 g/L, pH value = 3.0, experimental temperature = 298 K, contact time = 24 h.

Table 3. Elemental composition of CS₂C@SBA-3 before adsorption and after adsorption.

Adsorbent	Elemental Composition ^a (wt %)					
	C	Si	O	N	S	V
CS ₂ C@SBA-3 before adsorption	55.2	4.5	32.7	5.5	1.8	0.0
CS ₂ C@SBA-3 after adsorption ^b	46.3	5.8	32.6	2.7	0.4	12.2

^a determined by EDS. ^b Conditions: V(V) initial concentration = 100 ppm, CS₂C@SBA-3 dosage = 1.0 g/L, pH value = 3.0, experimental temperature = 298 K, contact time = 24 h.

FTIR and XPS measurement was further conducted to uncover the deeper mechanisms at work. Figure 9A–F reveals the results of FTIR spectra and XPS spectra of CS₂C@SBA-3 before and after the reaction with V(V). The bands stretching at 3454, 2924, 2854, 1632 and 1465 cm⁻¹ represents the presence of –OH/–NH₂/–SH, –CH₃, –CH₂, –CNH, and –C=S, respectively, on CS₂C@SBA-3 after the reaction (Figure 9A) [49–51]. Figure 9B, Figures S7 and S8 show the XPS survey spectra of CS₂C@SBA-3 before and after the reaction. Comparing these two XPS results, there was a distinct signal of V 2p at 516.8 eV which could prove the adsorption of V(V) on the surface of CS₂C@SBA-3 (Figure 9B) [39]. To illustrate the mechanism of the reduction of V(V) by CS₂C@SBA-3, XPS spectra of V 2p, V 2p_{1/2} and V 2p_{2/3} are provided in Figure 9C, D and E, respectively. There were three peaks at binding energies of 524.0, 516.8, and 513.3 eV, which occupied 26.9%, 66.9% and 6.6% of peak area, respectively (Figure 9C). The three peaks in XPS spectra of V 2p were characteristic of V₂O₅, V(IV), and V(III) respectively [52,53]. The results indicated that 73.1% of V(V) was reduced to V(IV) and V(III) on the surface of CS₂C@SBA-3 (Figure 9C–E).

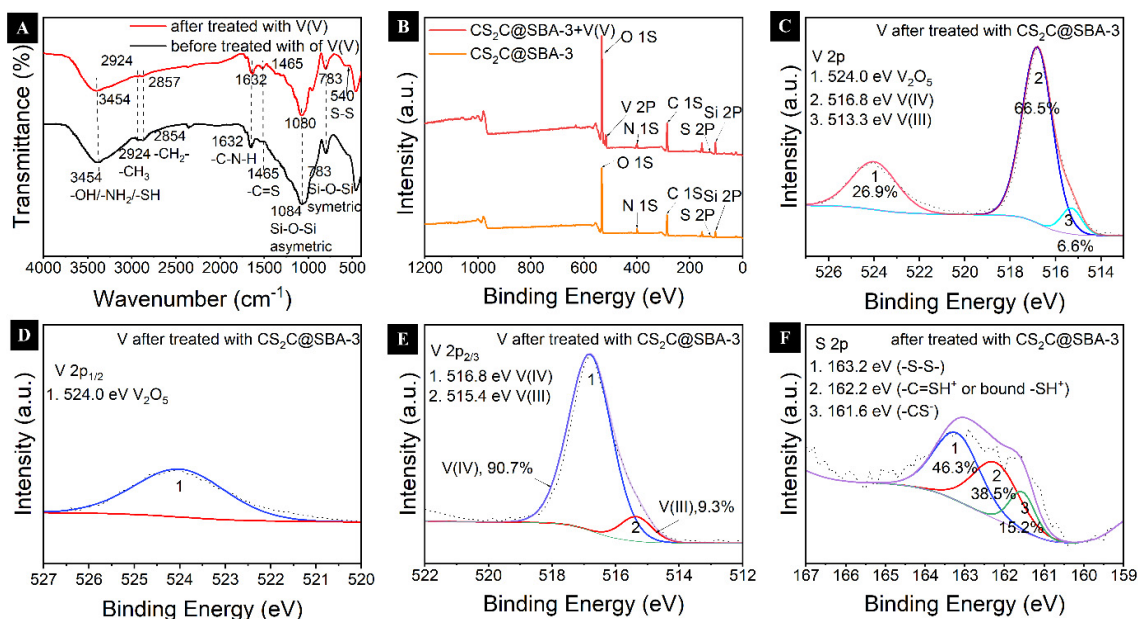


Figure 9. FTIR spectra of CS₂C@SBA-3 before and after adsorption (A). The XPS survey spectra of CS₂C@SBA-3 before and after adsorption (B). V 2p (C), V 2p_{1/2} (D), and V 2p_{2/3} (E). The XPS high-resolution of S 2p (F).

The successful synthesis of CS₂C@SBA-3 introduced organic functional groups including –SH, –OH, –NH₂ to the composite which can enable the adsorption coupled reduction of V(V). Figures 1D and 9F demonstrate the results of the XPS spectra of S 2p before and after the elimination of V(V), respectively. Before the reaction with V(V), S 2p XPS peaks at 163.1 and 161.8 eV could be attributed to the sulphur species of CS₂-chitosan including –C=S and –CS– respectively (Figure 1D). Their distribution molar percentages were 51.2% and 48.8%. After the reaction with V(V), a new S 2p XPS peak appeared at 163.2 eV (46.3%) which was attributed to the oxidation of –SH to disulfide bonds (–S–S–)

(Figure 9F) [21]. The weak peak at 540 cm^{-1} in FTIR spectra also confirmed the formation of disulfide bonds (Figure 9A) [49,54]. The results suggested that thiol functional groups on the surface of $\text{CS}_2\text{C@SBA-3}$ donated electrons to V(V) for its reduction. Meanwhile, a new peak appeared at 162.2 eV (38.5%) accounting for the protonated $-\text{C}=\text{SH}^+$ or $-\text{SH}_2^+$ due to the doping of H^+ on dithiocarbamate (Figure 9F). The formation of protonated sulphur species $-\text{C}=\text{SH}^+$ or $-\text{SH}_2^+$ would foster the electrostatic attraction between the residual V(V) anions and $\text{CS}_2\text{C@SBA-3}$, facilitating the nearly total elimination of V(V) .

To identify other factors which might support the elimination of V(V) , N 1s and O 1s XPS spectra were de-convoluted. Figure 10A–D show the XPS spectra of N 1s and O 1s before and after the elimination of V(V) . Before the reaction with V(V) , N 1s XPS peaks appearing at binding energies of 402.4, 400.2 and 399.3 eV could be associated to N– SiO_2 , $-\text{NH}_2$ and $-\text{NH}-$, respectively (Figure 10A) [55]. After the reaction with V(V) , the corresponding binding energies of N 1s peaks changed to 401.5, 399.4 and 398.7 eV, respectively (Figure 10B). The relative amounts of N– SiO_2 and $-\text{NH}_2$ increased from 4.4% and 15.0% to 41.5% and 55.3%, respectively. In contrast to the two functional groups, the relative amount of $-\text{NH}-$ dramatically decreased from 80.6% to 3.2% after the elimination of V(V) . The results suggest that large amounts of V(V) occupied $-\text{NH}-$. We could conclude that $-\text{NH}-$ constituted the dominant adsorption site for V(V) among the nitrogen functional groups. Furthermore, O 1s XPS spectra located at binding energies of 533.4, 532.6 and 531.8 eV corresponded to C–O–C, $-\text{CH}_2\text{OH}$ and $-\text{C}-\text{O}-\text{Si}$, respectively (Figure 10C,D) [56]. The new peak at 529.8 eV indicated the presence of V_2O_5 , as illustrated in Figure 9D [53]. After the elimination of V(V) , the relative density of $-\text{OH}$ decreased from 57.6% to 51.5%. The decrease of the density of $-\text{OH}$ was most likely attributable to the formation of hydrogen bonds between the V species and hydroxyl groups. As discussed above, the reaction between the $\text{CS}_2\text{C@SBA-3}$ and V(V) species is a catalytic reduction process in which most of V(V) (73.1%) is reduced into V(IV) and V(III) species which are less toxic. A small amount of V(V) was transformed into V(V) oxide, V_2O_5 . Meanwhile, the abundance of functional groups $-\text{NH}-$ enhanced the adsorption between vanadium species and $\text{CS}_2\text{C@SBA-3}$. The functional group $-\text{SH}$ is the dominant reactive site for reducing V(V) and was oxidized into disulfide bonds ($-\text{S}-\text{S}-$) in this catalytic reduction process.

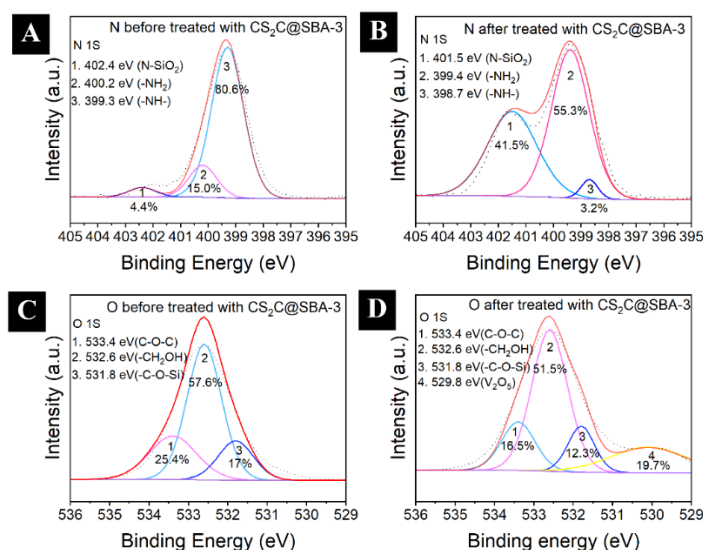


Figure 10. The XPS high-resolution of N 1s of $\text{CS}_2\text{C@SBA-3}$ before adsorption (A), and after adsorption (B). The XPS high-resolution of O 1s of $\text{CS}_2\text{C@SBA-3}$ before adsorption (C), and after adsorption (D). Conditions: V(V) initial concentration = 100 ppm, $\text{CS}_2\text{C@SBA-3}$ dosage = 1.0 g/L, pH value = 3.0, experimental temperature = 298 K, contact time = 24 h.

2.8. Recycling Application

As recyclability is one of the most important factors to judge the practical potential of these findings, a series of recycling application experiments were conducted. Figure 11 shows the removal efficiency of V(V) in five consecutive adsorption–desorption cycles. The removal efficiency of V(V) by CS₂C@SAB–3 decreased from 98.2% to 90.8% from the first to the fifth cycle of application. The results suggested that a V(V) removal up to 90.0% could be achieved after five adsorption–desorption cycles. Thus, CS₂C@SAB–3 can be regarded as a promising composite for the elimination of V(V) via catalytic reduction coupled adsorption process with satisfying reusability and good practical potential.

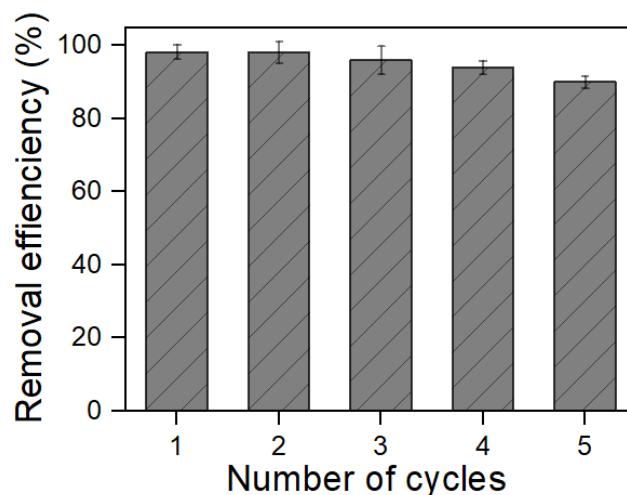


Figure 11. Effects of recyclability of CS₂C@SBA–3 on V(V) removal. Condition: V(V) initial concentration = 100 ppm, CS₂C@SBA–3 dosage = 1.0 g/L, pH value = 3.0, experimental temperature = 298 K, contact time = 24 h.

3. Materials and Methods

3.1. Materials

Deionized water (DI water, 18.2 MΩ·cm^{−1}) was obtained from Lichen water purifier UPTA. Chitosan was purchased from Meryer (Shanghai, China) without any purification. NaOH (≥96.0%), HCl (38.0%), NH₃·H₂O (28%), Na₃PO₄·12H₂O (98%), NaNO₃ (99.0%), NaHCO₃ (≥99.8%), Na₂S₂O₃ (99%) and CS₂ (99.9%) were purchased from Hushi (Shanghai, China). Glutaraldehyde (50% *v/v*) and sodium metavanadate (NaVO₃, 99.9%) were obtained from Aladdin. All the chemicals mentioned above were used at analytical grade without further purification.

3.2. Preparation of SBA-15, CS₂–Chitosan and CS₂C@SBA

SBA-15 and modified dithiocarbamate chitosan (CS₂-Chitosan) was synthesized based on the methods in previous literature [49]. Details can be found in Texts S1 and S2 respectively. CS₂C@SBA was synthesized by the following method. Initially, 0.60 g CS₂-chitosan was dissolved in 100 mL acetic acid solution (1.2% *v/v*). Then, different dosages of SBA-15 were added (mass ratios SBA-15: CS₂-chitosan = 1:2, 1:1 and 2:1). According to these mass ratios, CS₂C@SBA composites are named as CS₂C@SBA–1, CS₂C@SBA–2 and [57,58] CS₂C@SBA–3, respectively. Afterwards, the above mixture was stirred for 30 min at 313 K, followed by the addition of 0.50 mL glutaraldehyde (50.0% *v/v*) and further stirred for 2 h. After that, the pH of the mixture was adjusted to 9.0 by adding 0.1M NaOH, and stirred for 30 min. Finally, the solid suspension was filtered, washed several times with distilled water and dried at 333 K overnight.

3.3. Characterizations

Fourier Transform Infrared Spectra (FTIR) was measured by Nicolet 5700 spectrometer through the KBr pellet method over a wavelength range from 400 to 4000 cm^{-1} under a 4 cm^{-1} resolution. The Scanning Electron Microscopy (SEM) was performed on SEM Virion 200 combined with an electron dispersive X-ray (EDS) analyzer. The Transmission Electron Microscopy (TEM) was conducted on JEM-2100. The elemental composition (C, H, N and S wt%) of the materials was analyzed by Vario MICRO cube elemental analyzer (German). The Brunauer–Emmett–Teller (BET) pore properties of materials were measured via Belsorp–minill. Before the N_2 adsorption–desorption measurement, the composite was dried and degassed at 373 K under vacuum for 24 h. The X-ray diffraction (XRD, MiniFlex600, Japan) was conducted with radiation of Cu $\text{K}\alpha$ and scanning rate of 0.2°/min from 0.6° to 2.5° and 5°/min from 10° to 80°. Zeta potentials of the materials were measured by the Zetasizer Nano series at different pH (2.0–9.0). Firstly, 150 mg of composite was added into a plastic conical flask containing 65 mL DI water. Then the flask was mechanically shaken for 24 h. The resultant suspension was collected for zeta potentials determination in 0.01 mM NaCl solution. The pH was adjusted with 0.01 mM NaOH and HCl. The point of zero charge (pH_{ZPC}) was calculated by the zeta potentials under different pHs. The X-ray photoelectron spectroscopy (XPS) equipped with Al/Mg $\text{K}\alpha$ X-ray source with 30 eV pass energy in 0.5 eV step over an area of 650 mm \times 650 mm to the samples was carried out (ESCALAB 250Xi) at vacuum of 10^{-9} Torr, and the results were corrected by a reference of the C 1s peak from adventitious carbon at 284.8 eV and fitted with the Shirley method of background subtraction on XPSpeak4.1 Software.

3.4. Adsorption Experiments

The stock solution of V(V) (1000 ppm) was prepared by dissolving NaVO_3 with DI water. The effects of pH (2.0–10.0) on vanadium removal was conducted by adding 30 mg $\text{CS}_2\text{C@SBA}$ composites into 30 mL of V(V) solution (100 ppm) under stirring (200 rpm) at normal temperature for 24 h. The pH of solutions was adjusted by 0.1 M HCl and NaOH. The effect of adsorbent dosage was conducted in 25 mL V(V) solution (100 ppm) with varying adsorbent dosages (0.1, 0.3, 0.5, 1.0, 1.5 and 2 g/L). The kinetics experiment was conducted by adding 30 mg $\text{CS}_2\text{C@SBA}$ composites into 30 mL of V(V) solution (100 ppm) at pH 3.0 under stirring (200 rpm) at 298 K. The contact time was studied from 5 min to 12 h. The adsorption isotherm experiment was conducted by adjusting the concentration of V(V) from 10 to 500 ppm adding 1 g/L $\text{CS}_2\text{C@SBA}$ –3. In all experiments, the residual concentration of total V was measured by Inductively Coupled Plasma – Atomic Emission Spectroscopy (ICP–AES, Agilent 5110). Adsorption capacity (q_t) (mg/g) and percentage removal (%) were calculated by the following equations [41,59,60].

$$q_t = (C_0 - C_t) \frac{V}{m} \quad (1)$$

$$\% \text{Removal} = \frac{(C_0 - C_t)}{C_0} \times 100 \quad (2)$$

where C_0 and C_t are, respectively, the initial concentration and equilibrium concentration of total V (ppm); V is the solution volume (mL) while m is the adsorbent amount (g).

The results of the adsorption kinetic data were fitted by two models, pseudo–first–order, pseudo–second–order and Elovich models, as indicated below [10,61,62].

$$\ln(q_e - q_t) = \ln q_e - k_1 t \quad (3)$$

$$\frac{t}{q_t} = \frac{1}{k_2 q_e^2} + \frac{t}{q_e} \quad (4)$$

$$q_t = \frac{1}{\beta} \ln(1 + \partial \beta t) \quad (5)$$

where q_e and q_t are, respectively, the adsorbed capacity of V(V) on CS₂C@SBA-3 at equilibrium time and time t . k_1 (1/min) and k_2 (g/mg·min) are, respectively, the adsorption rate constants for pseudo-first-order and pseudo-second-order models. α (mg·min/g) is the initial rate constant and β (mg/g) is the desorption constant for Elovich model;

To determine the adsorption isotherm, Langmuir and Freundlich models are fitted to calculate the adsorption data, as indicated as the following equations [63]:

$$\frac{C_e}{q_e} = \frac{1}{q_m K_L} + \frac{C_e}{q_m} \quad (6)$$

$$\ln q_e = \ln K_f + \frac{1}{n} \ln C_e \quad (7)$$

where q_e and q_m are, respectively, the adsorption capacity at equilibrium and the maximum adsorption capacity of V(V) by CS₂C@SBA-3. C_e (ppm) is the concentration of V(V) at equilibrium. K_L (L/mg) and K_f ((mg/g)/(mg/L)^{1/n}) are, respectively, the Langmuir and Freundlich constants.

3.5. Regeneration and Recycle Experiments

To explore the recyclability of the material, the desorption was performed by using 25 mL NaOH solution (0.50 M) as the eluent at 298 K with 1 g/L CS₂C@SBA-3, and then using 0.01 M Na₂S₂O₃ solution to regenerate the oxidized disulfide bonds. The regenerated CS₂C@SBA-3 was employed to eliminate V(V) again, followed by the regeneration procedures. The experiment was repeated for five cycles. During the recycle experiments, the removal of V(V) was measured.

3.6. Effects of Groundwater Impurities

To investigate the effects of co-existing anions (60 ppm PO₄³⁻, 600 ppm SO₄²⁻, 400 ppm NO₃⁻, 400 ppm HCO₃⁻) and 60 ppm Cu²⁺, based on the typical concentration of common ions in ground water, 1 g/L CS₂C@SBA-3 was tested in 100 ppm V(V) solution at pH 3.0 for 24 h at 298 K. The effects of ionic strength were studied in 100 ppm V(V) solution at pH 3.0 for 24 h at 298 K with varying NaCl concentrations (10, 100 and 300 mM).

3.7. V(V) Elimination Assays in Spiked Real Water

The applicability of the adsorbent was also tested in spiked real water samples (10 ppm V(V)) including lake water, pond water and tap water collected from Wuhan at pH 3.0 and at their local pH 8.0. The physical and chemical properties of these samples are listed in Table S2.

4. Conclusions

In this study, dithiocarbamate chitosan modified SBA-15 (CS₂C@SBA) was successfully synthesized via a facile and robust procedure. Among the three CS₂C@SBA composites, CS₂C@SBA-3 which embraced the highest mass ratio of dithiocarbamate chitosan showed the most efficient performance in the elimination of V(V). At 298 K, a V(V) removal efficiency of 98.2% was achieved by 1 g/L CS₂C@SBA-3 in a solution containing 100 ppm of V(V). In that case, the adsorption capacity by CS₂C@SBA-3 was 218.00 mg/g. The adsorption kinetics fitted better with pseudo-second-order model ($R^2 = 0.9999$), indicating that the elimination of V(V) by CS₂C@SBA-3 was primarily triggered by chemisorption. The adsorption isotherm followed the Langmuir model ($R^2 = 0.9981$), revealing the monolayer adsorption on the surface of CS₂C@SBA-3. FTIR, SEM-EDS and XPS characterization results demonstrated that the functional group -SH played a vital role, acting as a proton-coupled electron donor to reduce 73.5% V(V) into V(IV) and V(III) and transformed residual V(V) into V(V) oxide V₂O₅. Via the reduction of high-valent vanadium, its toxicity was reduced significantly. Furthermore, CS₂C@SBA-3 displayed high selectivity towards V(V) elimination in the presence of various co-existing ions in synthetic and spiked real water samples which could be attributed to the abundant -NH- on its surface.

Hence, we can conclude that CS₂C@SBA-3 is a promising composite to eliminate V(V) via an adsorption coupled catalytic reduction mechanism, with good practical potentials. CS₂C@SBA-3 can be applied in the reductive elimination of high-valent heavy metals in efficient remediation of water pollution.

Supplementary Materials: The following supporting information can be downloaded at: <https://www.mdpi.com/article/10.3390/catal12111469/s1>, Text S1: Details of synthesis procedures of SBA-15; Text S2: Details of synthesis procedures of CS₂-chitosan; Figure S1: Nitrogen sorption isotherms of SBA-15 and CS₂C@SBA-3; Figure S2: The XRD patterns of preparation composite; Figure S3: TEM images of SBA-15 and CS₂C@SBA-3; Figure S4: SEM images of CS₂C@SBA-3 after reaction with V(V); Figure S5: EDS elemental mapping images of CS₂C@SBA-3 before reaction with V(V); Figure S6: EDS elemental mapping images of CS₂C@SBA-3 after reaction with V(V); Figure S7: The XPS survey spectra of CS₂C@SBA-3 before reaction; Figure S8: The XPS survey spectra of CS₂C@SBA-3 after reaction; Table S1: Porous properties of SBA-15 and CS₂C@SBA-3; Table S2: Physico-chemical properties of water samples used in this study.

Author Contributions: Y.H.: Data curation, Methodology, Validation, Investigation, Writing—original draft. J.W.: Methodology, Supervision, Writing—review and editing. M.L.: Methodology. Z.Y.: Funding acquisition, Supervision. All authors have read and agreed to the published version of the manuscript.

Funding: This work was financially supported by the National Natural Science Foundation of China (No. 21573163) and the Natural Science Foundation of Hubei Province (No. 2015CFA017).

Acknowledgments: We thank the Analytical and Testing Centre of Wuhan University for help with the characterization.

Conflicts of Interest: The authors declare that they have no known competing financial interests or personal relationships that could have appeared to influence the work reported in this paper.

Abbreviations

Santa Barbara Amorphous type 15 material (SBA-15); Dithiocarbamate chitosan (CS₂-chitosan); Dithiocarbamate chitosan modified SBA-15 (CS₂C@SBA); Vanadium(V) [V(V)]; Fourier Transform Infrared Spectra (FTIR); Scanning Electron Microscopy with an electron dispersive X-ray (SEM-EDS); Brunauer-Emmett-Teller (BET); X-ray diffraction (XRD); Transmission Electron Microscopy (TEM); X-ray photoelectron spectroscopy (XPS).

References

1. Wang, Z.L.; Zhang, B.G.; He, C.; Shi, J.X.; Wu, M.X.; Guo, J.H. Sulfur-based Mixotrophic Vanadium (V) Bio-reduction towards Lower Organic Requirement and Sulfate Accumulation. *Water Res.* **2021**, *189*, 116655. [[CrossRef](#)] [[PubMed](#)]
2. Wang, P.; Hu, J.; Wang, Y.D.; Liu, T.Y. Enhanced elimination of V⁵⁺ in wastewater using zero-valent iron activated by ball milling: The overlooked crucial roles of energy input and sodium chloride. *J. Hazard. Mater.* **2022**, *435*, 129050. [[CrossRef](#)]
3. Sun, F.J.; Liu, M.; Yuan, B.; He, J.; Wu, P.; Liu, C.J.; Jiang, W. Separation of vanadium and chromium by selective adsorption by titanium-based microspheres. *Chem. Eng. J.* **2022**, *450*, 138039. [[CrossRef](#)]
4. Aregay, G.G.; Ali, J.; Shahzad, A.; Ifthikar, J.; Oyekunle, D.T.; Chen, Z. Application of layered double hydroxide enriched with electron rich sulfide moieties (S₂O₄⁽²⁻⁾) for efficient and selective removal of vanadium (V) from diverse aqueous medium. *Sci. Total Environ.* **2021**, *792*, 148543. [[CrossRef](#)] [[PubMed](#)]
5. Schiffer, S.; Liber, K. Toxicity of aqueous vanadium to zooplankton and phytoplankton species of relevance to the athabasca oil sands region. *Ecotoxicol. Environ. Saf.* **2017**, *137*, 1–11. [[CrossRef](#)] [[PubMed](#)]
6. Wang, H.S.; Chen, N.; Feng, C.P.; Deng, Y. Synchronous microbial V(V) reduction and denitrification using corn straw as the sole carbon source. *Sci. Total Environ.* **2022**, *839*, 156343. [[CrossRef](#)]
7. Chen, L.; Liu, J.R.; Hu, W.F.; Gao, J.; Yang, J.Y. Vanadium in soil-plant system: Source, fate, toxicity, and bioremediation. *J. Hazard. Mater.* **2021**, *405*, 124200. [[CrossRef](#)]
8. Zhu, X.B.; Li, W.; Zhang, Q.; Zhang, C.X.; Chen, L.J. Separation characteristics of vanadium from leach liquor of red mud by ion exchange with different resins. *Hydrometallurgy* **2018**, *176*, 42–48. [[CrossRef](#)]
9. Zhang, B.G.; Li, Y.N.; Fei, Y.M.; Cheng, Y.T. Novel Pathway for Vanadium(V) Bio-Detoxification by Gram-Positive *Lactococcus raffinolactis*. *Environ. Sci. Technol.* **2021**, *55*, 2121–2131. [[CrossRef](#)] [[PubMed](#)]

10. Zhang, R.C.; Leiviska, T. Surface modification of pine bark with quaternary ammonium groups and its use for vanadium removal. *Chem. Eng. J.* **2020**, *385*, 123967. [[CrossRef](#)]
11. Kong, X.; Chen, J.; Tang, Y.; Lv, Y.; Chen, T.; Wang, H. Enhanced removal of vanadium(V) from groundwater by layered double hydroxide-supported nanoscale zerovalent iron. *J. Hazard. Mater.* **2020**, *392*, 122392. [[CrossRef](#)] [[PubMed](#)]
12. Kong, D.; Foley, S.R.; Wilson, L.D. An Overview of Modified Chitosan Adsorbents for the Removal of Precious Metals Species from Aqueous Media. *Molecules* **2022**, *27*, 978. [[CrossRef](#)] [[PubMed](#)]
13. Kazachenko, A.S.; Akman, F.; Malyar, Y.N.; Issaoui, N.; Vasilieva, N.Y.; Karacharov, A.A. Synthesis optimization, DFT and physicochemical study of chitosan sulfates. *J. Mol. Struct.* **2021**, *1245*, 131083. [[CrossRef](#)]
14. Crini, G.; Lichtfouse, E.; Wilson, L.D.; Morin-Crini, N. Conventional and non-conventional adsorbents for wastewater treatment. *Environ. Chem. Lett.* **2019**, *17*, 195–213.
15. Steiger, B.G.K.; Wilson, L.D. Modular Chitosan-Based Adsorbents for Tunable Uptake of Sulfate from Water. *Int. J. Mol. Sci.* **2020**, *21*, 7130. [[CrossRef](#)]
16. Nuryono, N.; Miswanda, D.; Sakti, S.C.W.; Rusdiarso, B.; Krisbiantoro, P.A.; Utami, N.; Otomo, R.; Kamiya, Y. Chitosan-functionalized natural magnetic particle@silica modified with (3-chloropropyl)trimethoxysilane as a highly stable magnetic adsorbent for gold(III) ion. *Mater. Chem. Phys.* **2020**, *255*, 123507. [[CrossRef](#)]
17. Zhuang, S.T.; Zhu, K.K.; Wang, J.L. Fibrous chitosan cellulose composite as an efficient adsorbent for Co(II) removal. *J. Clean. Prod.* **2021**, *285*, 124911. [[CrossRef](#)]
18. Bui, T.H.; Lee, W.; Jeon, S.B.; Kim, K.W.; Lee, Y. Enhanced Gold(III) adsorption using glutaraldehyde-crosslinked chitosan beads: Effect of crosslinking degree on adsorption selectivity, capacity, and mechanism. *Sep. Purif. Technol.* **2020**, *248*, 116989.
19. Bilican, I.; Pekdemir, S.; Onses, M.S.; Akyuz, L.; Altuner, E.M.; Koc-Bilican, B.; Zang, L.S.; Mujtaba, M.; Mulercikas, P.; Kaya, M. Chitosan Loses Innate Beneficial Properties after Being Dissolved in Acetic Acid: Supported by Detailed Molecular Modeling. *ACS Sustain. Chem. Eng.* **2020**, *8*, 18083–18093. [[CrossRef](#)]
20. Yin, Z.; Qiu, D.; Zhang, M.Y. Molecular level study of cadmium adsorption on dithiocarbamate modified chitosan. *Environ. Pollut.* **2021**, *271*, 116322. [[CrossRef](#)] [[PubMed](#)]
21. Ifthikar, J.; Chen, Z.; Chen, Z.; Jawad, A. A self-gating proton-coupled electron transfer reduction of hexavalent chromium by core-shell SBA-Dithiocarbamate chitosan composite. *J. Hazard. Mater.* **2020**, *384*, 121257. [[CrossRef](#)]
22. Ifthikar, J.; Zhao, M.; Shahzad, A.; Shahib, I.I.; Wang, J.; Wang, H.B.; Sellaoui, L.; Chen, Z.Q.; Chen, Z.L. Recyclable process modeling study of hexavalent chromium elimination by thiol-based electron donor: Implications for practical applicability. *J. Environ. Chem. Eng.* **2021**, *9*, 105645. [[CrossRef](#)]
23. Roncevic, S.; Nemet, I.; Ferri, T.Z.; Matkovic-Calogovic, D. Characterization of nZVI nanoparticles functionalized by EDTA and dipicolinic acid: A comparative study of metal ion removal from aqueous solutions. *RSC Adv.* **2019**, *9*, 31043–31051. [[CrossRef](#)] [[PubMed](#)]
24. Ifthikar, J.; Jiao, X.; Ngambia, A.; Wang, T.; Khan, A.; Jawad, A.; Xue, Q.; Liu, L.; Chen, Z. Facile One-Pot Synthesis of Sustainable Carboxymethyl Chitosan – Sewage Sludge Biochar for Effective Heavy Metal Chelation and Regeneration. *Bioresour. Technol.* **2018**, *262*, 22–31. [[CrossRef](#)]
25. Verma, P.; Kuwahara, Y.; Mori, K.; Raja, R.; Yamashita, H. Functionalized mesoporous SBA-15 silica: Recent trends and catalytic applications. *Nanoscale* **2020**, *12*, 11333–11363. [[CrossRef](#)] [[PubMed](#)]
26. Qiao, Y.; Said, N.; Rauser, M.; Yan, K.; Qin, F.; Theyssen, N.; Leitner, W. Preparation of SBA-15 supported Pt/Pd bimetallic catalysts using supercritical fluid reactive deposition: How do solvent effects during material synthesis affect catalytic properties? *Green Chem.* **2017**, *19*, 977–986. [[CrossRef](#)]
27. Kazachenko, A.S.; Akman, F.; Vasilieva, N.Y.; Issaoui, N.; Malyar, Y.N.; Kondrasenko, A.A.; Borovkova, V.S.; Miroshnikova, A.V.; Kazachenko, A.S.; Al-Dossary, O.; et al. Catalytic Sulfation of Betulin with Sulfamic Acid: Experiment and DFT Calculation. *Int. J. Mol. Sci.* **2022**, *23*, 1602. [[CrossRef](#)] [[PubMed](#)]
28. Kazachenko, A.S.; Akman, F.; Vasilieva, N.Y.; Malyar, Y.N.; Fetisova, O.Y.; Lutoshkin, M.A.; Berezhnaya, Y.D.; Miroshnikova, A.V.; Issaoui, N.; Xiang, Z.Y. Sulfation of Wheat Straw Soda Lignin with Sulfamic Acid over Solid Catalysts. *Polymers* **2022**, *14*, 3000. [[CrossRef](#)] [[PubMed](#)]
29. Kazachenko, A.; Akman, F.; Medimagh, M.; Issaoui, N.; Vasilieva, N.; Malyar, Y.N.; Sudakova, I.G.; Karacharov, A.; Miroshnikova, A.; Al-Dossary, O.M. Sulfation of Diethylaminoethyl-Cellulose: QTAIM Topological Analysis and Experimental and DFT Studies of the Properties. *ACS Omega* **2021**, *6*, 22603–22615. [[CrossRef](#)]
30. Zhang, L.; Guo, D.; Tantai, X.; Jiang, B.; Sun, Y.; Yang, N. Synthesis of Three-Dimensional Hierarchical Flower-Like Mg–Al Layered Double Hydroxides with Excellent Adsorption Performance for Organic Anionic Dyes. *Trans. Tianjin Univ.* **2020**, *27*, 394–408. [[CrossRef](#)]
31. Hongmanorom, P.; Ashok, J.; Zhang, G.H.; Bian, Z.F.; Wai, M.H.; Zeng, Y.Q.; Xi, S.B.; Borgna, A.; Kawi, S. Enhanced performance and selectivity of CO₂ methanation over phyllosilicate structure derived Ni-Mg/SBA-15 catalysts. *Appl. Catal. B-Environ.* **2021**, *282*, 119564. [[CrossRef](#)]
32. Alkafajy, A.M.; Albayati, T.M. High performance of magnetic mesoporous modification for loading and release of meloxicam in drug delivery implementation. *Mater. Today Commun.* **2020**, *23*, 100890. [[CrossRef](#)]
33. Betiha, M.A.; Moustafa, Y.M.; El-Shahat, M.F.; Rafik, E. Polyvinylpyrrolidone–Aminopropyl–SBA-15 schiff Base hybrid for efficient removal of divalent heavy metal cations from wastewater. *J. Hazard. Mater.* **2020**, *397*, 122675. [[CrossRef](#)] [[PubMed](#)]

34. Daoura, O.; Fornasieri, G.; Boutros, M.; El Hassan, N.; Beaunier, P.; Thomas, C.; Selmane, M.; Miche, A.; Sassoie, C.; Ersen, O.; et al. One-pot prepared mesoporous silica SBA-15-like monoliths with embedded Ni particles as selective and stable catalysts for methane dry reforming. *Appl. Catal. B-Environ.* **2021**, *280*, 119417. [[CrossRef](#)]
35. Shimon, D.; Chen, C.H.; Lee, J.J.; Didas, S.A.; Sievers, C.; Jones, C.W.; Hayes, S.E. (15)N Solid State NMR Spectroscopic Study of Surface Amine Groups for Carbon Capture: 3-Aminopropylsilyl Grafted to SBA-15 Mesoporous Silica. *Environ. Sci. Technol.* **2018**, *52*, 1488–1495. [[CrossRef](#)]
36. Cao, T.; Li, Z.; Xiong, Y.; Yang, Y.; Xu, S.; Bisson, T.; Gupta, R.; Xu, Z. Silica–Silver Nanocomposites as Regenerable Sorbents for Hg(0) Removal from Flue Gases. *Environ. Sci. Technol.* **2017**, *51*, 11909–11917. [[CrossRef](#)]
37. Dong, W.C.; Liu, J.; Hao, J.M.; Zeng, Y. Adsorption of DTC–CTS on sphalerite (110) and Cu-activated sphalerite (110) surfaces: A DFT study. *Appl. Surf. Sci.* **2021**, *551*, 149466. [[CrossRef](#)]
38. Ifthikar, J.; Shahib, I.I.; Sellaoui, L.; Jawad, A.; Zhao, M.M.; Chen, Z.Q.; Chen, Z.L. pH tunable anionic and cationic heavy metal reduction coupled adsorption by thiol cross-linked composite: Physicochemical interpretations and fixed-bed column mathematical model study. *Chem. Eng. J.* **2020**, *401*, 126041. [[CrossRef](#)]
39. Ifthikar, J.; Wang, J.; Wang, Q.L.; Wang, T.; Wang, H.B.; Khan, A.; Jawad, A.; Sun, T.T.; Jiao, X.; Chen, Z.Q. Highly Efficient Lead Distribution by Magnetic Sewage Sludge Biochar: Sorption Mechanisms and Bench Applications. *Bioresour. Technol.* **2017**, *238*, 399–406. [[CrossRef](#)] [[PubMed](#)]
40. Dong, Y.B.; Lin, H.; Zhao, Y.M.; Menzembere, E. Remediation of vanadium-contaminated soils by the combination of natural clay mineral and humic acid. *J. Clean. Prod.* **2021**, *279*, 123874. [[CrossRef](#)]
41. Gogoi, H.; Zhang, R.C.; Matusik, J.; Leiviska, T.; Ramo, J.; Tanskanen, J. Vanadium removal by cationized sawdust produced through iodomethane quaternization of triethanolamine grafted raw material. *Chemosphere* **2021**, *278*, 130445. [[CrossRef](#)] [[PubMed](#)]
42. Chen, L.; Zhu, Y.Y.; Luo, H.Q.; Yang, J.Y. Characteristic of adsorption, desorption, and co-transport of vanadium on humic acid colloid. *Ecotox. Environ. Safe.* **2020**, *190*, 110087. [[CrossRef](#)]
43. Zhu, X.B.; Li, W.; Zhang, C.X. Extraction and removal of vanadium by adsorption with resin 201*7 from vanadium waste liquid. *Environ. Res.* **2020**, *180*, 108865. [[CrossRef](#)] [[PubMed](#)]
44. Gan, C.D.; Liu, M.; Lu, J.; Yang, J.Y. Adsorption and Desorption Characteristics of Vanadium (V) on Silica. *Water Air Soil Poll.* **2020**, *231*, 10. [[CrossRef](#)]
45. He, C.; Zhang, B.G.; Lu, J.P.; Qiu, R. A newly discovered function of nitrate reductase in chemoautotrophic vanadate transformation by natural mackinawite in aquifer. *Water Res.* **2021**, *189*, 116664. [[CrossRef](#)]
46. Li, M.; Zhang, B.G.; Zou, S.Q.; Liu, Q.S.; Yang, M. Highly selective adsorption of vanadium (V) by nano-hydrous zirconium oxide-modified anion exchange resin. *J. Hazard. Mater.* **2020**, *384*, 121386. [[CrossRef](#)]
47. Zhang, B.G.; Jiang, Y.F.; Zuo, K.C.; He, C.; Dai, Y.R.; Ren, Z.J. Microbial vanadate and nitrate reductions coupled with anaerobic methane oxidation in groundwater. *J. Hazard. Mater.* **2020**, *382*, 121228. [[CrossRef](#)]
48. Aregay, G.G.; Ali, J.; Du, Y.S.; Shahzad, A.; Chen, Z.Q. Efficient and selective removal of chromium (VI) by sulfide assembled hydrotalcite compounds through concurrent reduction and adsorption processes. *J. Mol. Liq.* **2019**, *294*, 111532. [[CrossRef](#)]
49. Yong, S.K.; Skinner, W.M.; Bolan, N.S.; Lombi, E.; Kunhikrishnan, A.; Ok, Y.S. Sulfur crosslinks from thermal degradation of chitosan dithiocarbamate derivatives and thermodynamic study for sorption of copper and cadmium from aqueous system. *Environ. Sci. Pollut. Res.* **2016**, *23*, 1050–1059. [[CrossRef](#)]
50. Kazachenko, A.S.; Vasilieva, N.Y.; Fetisova, O.Y.; Sychev, V.V.; Elsuif'ev, E.V.; Malyar, Y.N.; Issaoui, N.; Miroshnikova, A.V.; Borovkova, V.S.; Kazachenko, A.S.; et al. New reactions of betulin with sulfamic acid and ammonium sulfamate in the presence of solid catalysts. *Biomass Convers. Biorefinery* **2022**. [[CrossRef](#)]
51. Kazachenko, A.S.; Akman, F.; Abdelmoulahi, H.; Issaoui, N.; Malyar, Y.N.; Al-Dossary, O.; Wojcik, M.J. Intermolecular hydrogen bonds interactions in water clusters of ammonium sulfamate: FTIR, X-ray diffraction, AIM, DFT, RDG, ELF, NBO analysis. *J. Mol. Liq.* **2021**, *342*, 117475. [[CrossRef](#)]
52. Fan, K.; Chen, H.; Ji, Y.; Huang, H.; Claesson, P.M.; Daniel, Q.; Philippe, B.; Rensmo, H.; Li, F.; Luo, Y.; et al. Nickel–vanadium monolayer double hydroxide for efficient electrochemical water oxidation. *Nat. Commun.* **2016**, *7*, 11981. [[CrossRef](#)] [[PubMed](#)]
53. Silversmit, G.; Depla, D.; Poelman, H.; Marin, G.B.; De Gryse, R. Determination of the V2p XPS binding energies for different vanadium oxidation states (V^{5+} to V^{0+}). *J. Electron Spectrosc. Relat. Phenom.* **2004**, *135*, 167–175. [[CrossRef](#)]
54. Brandt, N.N.; Chikishev, A.Y.; Kruzhillin, V.N. Raman study of the cleavage of disulphide bonds in albumin, chymotrypsin, and thrombin. *Vib. Spectrosc.* **2017**, *89*, 75–80. [[CrossRef](#)]
55. Das, S.; Chakraborty, P.; Ghosh, R.; Paul, S.; Mondal, S.; Panja, A.; Nandi, A.K. Folic Acid–Polyaniline Hybrid Hydrogel for Adsorption/Reduction of Chromium(VI) and Selective Adsorption of Anionic Dye from Water. *ACS Sustain. Chem. Eng.* **2017**, *5*, 9325–9337. [[CrossRef](#)]
56. Veerakumar, P.; Thanasekaran, P.; Lin, K.-C.; Liu, S.-B. Biomass Derived Sheet-like Carbon/Palladium Nanocomposite: An Excellent Opportunity for Reduction of Toxic Hexavalent Chromium. *ACS Sustain. Chem. Eng.* **2017**, *5*, 5302–5312. [[CrossRef](#)]
57. Kazachenko, A.S.; Medimagh, M.; Issaoui, N.; Al-Dossary, O.; Wojcik, M.J.; Kazachenko, A.S.; Miroshnikova, A.V.; Malyar, Y.N. Sulfamic acid/water complexes (SAA–H₂O((1–8))) intermolecular hydrogen bond interactions: FTIR, X-ray, DFT and AIM analysis. *J. Mol. Struct.* **2022**, *1265*, 133394. [[CrossRef](#)]
58. Levdansky, A.V.; Vasilyeva, N.Y.; Malyar, Y.N.; Kondrasenko, A.A.; Fetisova, O.Y.; Kazachenko, A.S.; Levdansky, V.A.; Kuznetsov, B.N. An Efficient Method of Birch Ethanol Lignin Sulfation with a Sulfaic Acid–Urea Mixture. *Molecules* **2022**, *27*, 6356. [[CrossRef](#)]

59. He, W.Y.; Liao, W.; Yang, J.Y.; Jeyakumar, P.; Anderson, C. Removal of vanadium from aquatic environment using phosphoric acid modified rice straw. *Bioremediation J.* **2020**, *24*, 80–89. [[CrossRef](#)]
60. Yang, J.Y.; Luo, H.Q.; Zhu, Y.Y.; Yu, Y.Q.; He, W.Y.; Wu, Z.Z.; Wang, B. Adsorption-desorption and co-migration of vanadium on colloidal kaolinite. *Environ. Sci. Pollut. R.* **2020**, *27*, 17910–17922. [[CrossRef](#)]
61. Yap, P.L.; Auyoong, Y.L.; Hassan, K.; Farivar, F.; Tran, D.N.H.; Ma, J.; Losic, D. Multithiol functionalized graphene bio-sponge via photoinitiated thiol-ene click chemistry for efficient heavy metal ions adsorption. *Chem. Eng. J.* **2020**, *395*, 124965. [[CrossRef](#)]
62. Abukhadra, M.R.; Bakry, B.M.; Adlii, A.; Yakout, S.M.; El-Zaidy, M.E. Facile conversion of kaolinite into clay nanotubes (KNTs) of enhanced adsorption properties for toxic heavy metals (Zn^{2+} , Cd^{2+} , Pb^{2+} , and Cr^{6+}) from water. *J. Hazard. Mater.* **2019**, *374*, 296–308. [[CrossRef](#)] [[PubMed](#)]
63. Shahat, A.; Hassan, H.M.A.; Azzazy, H.M.E.; El-Sharkawy, E.A.; Abdou, H.M.; Awual, M.R. Novel hierarchical composite adsorbent for selective lead(II) ions capturing from wastewater samples. *Chem. Eng. J.* **2018**, *332*, 377–386. [[CrossRef](#)]